Anisotropic Ballistic Transport through a Potential Barrier on Monolayer Phosphorene *

Fang Cheng(程芳)**, Bing He(何兵)

Department of Physics and Electronic Science, Changsha University of Science and Technology, Changsha 410004

(Received 22 February 2016)

We demonstrate theoretically the anisotropic quantum transport of electrons through a single barrier on monolayer phosphorene. Using an effective $\boldsymbol{k}\cdot\boldsymbol{p}$ Hamiltonian, we find that the transmission probability for transport through n–n–n (or n–p–n) junction is an oscillating function of the incident angle, the barrier height, as well as the incident energy of electrons. The conductance in such systems depends sensitively on the transport direction due to the anisotropic effective mass. By tuning the Fermi energy and gate voltage, the channels can be transited from opaque to transparent, which provides us with an efficient way to control the transport of monolayer phosphorene-based microstructures.

PACS: 73.22.−f, 73.63.−b, 68.65.−k DOI: 10.1088/0256-307X/33/5/057301

Recently, layered black phosphorus has attracted intensive attention due to its unique electronic properties and potential applications in nanoelectronics.[1–4] Black phosphorus differs from graphene in the electronic band structure. While graphene is a zero-gap semiconductor (the conduction and valence bands touch at the so-called Dirac or neutrality point), black phosphorus is a semiconductor with a sizeable gap. Black phosphorus possesses a direct band gap 0.3 eV located at the Z point.[5] This direct gap moves to Γ points and increases to 1.5–2 eV when the thickness decreases from bulk to a few layers and eventually a monolayer via mechanical exfoliation.[6] Hence, black phosphorus is an appealing candidate for tunable photodetection from the visible to the infrared part of the spectrum.[7] To date, various interesting properties for phosphorene have been predicted, particularly those related to strain-induced gap modification,[1] tunable optical properties,[8] layer-controlled anisotropic excitons.[9] Further, the field-effect-transistor (FET) based on few-layer black phosphorus is found to have an on/off ratio of 10^5 and a carrier mobility at room temperature as high as $10^3\,\mathrm{cm}^2/\mathrm{V{\cdot}s}$,[10,11] which make black phosphorus a favorable material for next-generation electronic devices.

The phosphorus atoms are not arranged in a completely planar lattice, but they form a puckered honeycomb lattice. This atomic arrangement yields two inequivalent directions within the black phosphorus lattice: the zigzag (parallel to the atomic ridges) and the armchair (perpendicular to the ridges). This strong structural anisotropy is the stem of its particular in-plane anisotropic electrical and optical properties.

There exists a large body of works on tunneling through potential barriers on graphene.[12] In this Letter, we study the anisotropic quantum transport of electrons through a single barrier on monolayer phosphorene. Using an effective $\boldsymbol{k}\cdot\boldsymbol{p}$ Hamiltonian, we find that the transmission probability for transport through n–n–n (or n–p–n) junction is an oscillating function of the incident angle, the barrier height, as well as the incident energy of electrons. The tunneling is forbidden when the incident angle exceeds a critical value. The critical angles for tunneling electrons transporting along different directions, as the different effective masses along the Γ–X direction and the Γ–Y direction, are different. Interestingly, owing to the anisotropic energy dispersions, i.e., the effective masses, the conductance shows strong anisotropic behavior.

We consider a monolayer of phosphorene with an electrostatic potential barrier. The electrostatic potentials can be tuned by changing the applied voltages (see Fig. 1). The low energy physics of monolayer black phosphorus around Γ points can be well described by an anisotropic two-band $\boldsymbol{k}\cdot\boldsymbol{p}$ model,[1]

$$H=\begin{pmatrix} E_{\mathrm{c}}+V_j+\alpha k_x^2+\beta k_y^2 & \gamma k_x \\ \gamma k_x & E_{\mathrm{v}}+V_j-\lambda k_x^2-\eta k_y^2 \end{pmatrix}, \tag{1}$$

which agrees well with the tight binding (TB) model.[13] Here $E_{\mathrm{c}}=0.34\,\mathrm{eV}$ ($E_{\mathrm{v}}=-1.18\,\mathrm{eV}$) is the conduction (valence) band edge, V_j is the height of the electrostatic barrier for the jth region, $\gamma=-5.2305\,\mathrm{eV{\cdot}\AA}$ describes the interband coupling between the conduction and valence band. The parameters α, β, λ and η are related to the effective masses with $\alpha=\hbar^2/2m_{cx}$, $\beta=\hbar^2/2m_{cy}$, $\lambda=\hbar^2/2m_{vx}$, $\eta=\hbar^2/2m_{vy}$. Here $m_{cx}=0.793m_{\mathrm{e}}$, $m_{cy}=0.848m_{\mathrm{e}}$, $m_{vx}=1.363m_{\mathrm{e}}$, $m_{vy}=1.142m_{\mathrm{e}}$, and m_{e} is the free

*Supported by the National Natural Science Foundation of China under Grant No 11374002, the Hunan Provincial Natural Science Foundation of China under Grant No 13JJ2026, the Scientific Research Fund of Hunan Provincial Education Department under Grant No 12B010, the Science and Technology Innovative Research Team in Higher Educational Institutions of Hunan Province, and the Construct Program of the Key Discipline in Hunan Province.

**Corresponding author. Email: chengfangg@gmail.com

© 2016 Chinese Physical Society and IOP Publishing Ltd

electron mass. As indicated in Fig. 1, the electrostatic potential is assumed to be zero in regions I and III and $V_j = V$ in region II.

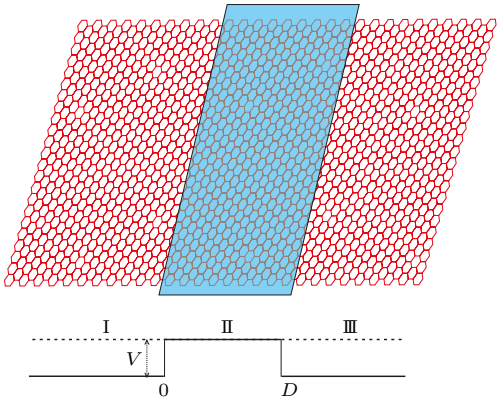

Fig. 1. Schematic diagram of a single barrier geometry on monolayer phosphorene. The shaded regions denote the regions below the electric gates. The lower panel describes the potential profile.

Although the dispersion is dominated by the off-diagonal element, we can decouple the conduction and valence band in a low-energy regime due to the large optical gap (1.52 eV), i.e., the weak interband coupling. The role of the off-diagonal elements can be taken into account perturbatively. The decoupled Hamiltonian reads[14]

$$H = \begin{pmatrix} H_{11} & 0 \\ 0 & H_{22} \end{pmatrix}, \tag{2}$$

where $H_{11} = E_{\rm c} + V_j + \alpha' k_x^2 + \beta k_y^2$, $H_{22} = E_{\rm v} + V_j - \lambda' k_x^2 - \eta k_y^2$, $\alpha' = \alpha + \gamma^2/E_{\rm g}$, $\lambda' = \lambda + \gamma^2/E_{\rm g}$, and $E_{\rm g} = E_{\rm c} - E_{\rm v}$ is the energy gap. Owing to the interband coupling, the effective masses around Γ points along the k_x direction are modified as

$$m^\star_{cx} = \frac{\hbar^2}{2\alpha'} = 0.167 m_{\rm e},\ m^\star_{vx} = \frac{\hbar^2}{2\lambda'} = 0.184 m_{\rm e}. \tag{3}$$

However, the effective masses around Γ points along the k_y direction remain unchanged with

$$m^\star_{cy} = \frac{\hbar^2}{2\beta} = 0.848 m_{\rm e},\ m^\star_{vy} = \frac{\hbar^2}{2\eta} = 1.142 m_{\rm e}. \tag{4}$$

We start by investigating electron tunneling through an electric n–n or n–p junction in monolayer phosphorene, with $V_{\rm in} = 0$ in region I ($x < 0$) and $V_{\rm out} = V$ in region II ($0 < x < D$), as shown in Fig. 1. We model the electrostatic potential of a p–n junction by a step-like potential. This idealized model can give the essential features of the quantum tunneling. A smoother experimentally realizable potential profile would not change the main results.

We consider two cases of transport: one is along Γ–X (zigzag) and the other is along the Γ–Y (armchair) direction in single-layer phosphorene. For the transport along the Γ–X direction, the translational invariance along the y direction gives rise to the conservation of k_y, and thus the solutions to Eq. (2) in jth region can be written as $\Psi_j(x,y) = \Psi_j(x)\exp(ik_y y)$. The wavevector k satisfies the relationship $k_{cx}^2 = \frac{(E-E_{\rm c})}{\alpha'} - \frac{\beta}{\alpha'}k_y^2$, and $k_{vx}^2 = \frac{(E_{\rm v}-E)}{\lambda'} - \frac{\eta}{\lambda'}k_y^2$, where k_{cx} (k_{vx}) denotes the longitudinal wavevector of the conductance (valence) band. Continuity of the wave functions and the first derivative of the wave functions at $x = 0$ gives the transmission coefficient t. Since the modes in n- and p-doped regions have different group velocities, the transmission probability is given by $T = (v_{\rm out}/v_{\rm in})|t|^2$, where $v_i = \frac{1}{\hbar}\partial(E_{\rm F} - V_j)/\partial k_x^j$ for propagating states and $v_i = 0$ for evanescent states. We can also define the incident and refractive angles for electrons in propagating states in $\theta_0 = \arctan(k_y/k_x)$ and $\theta = \arctan(k_y/k'_x)$. Here θ_{0c} is analogous to the critical angle for total reflection in optics,

$$\theta_{0c} = \arctan\left(\sqrt{\frac{E - E_{\rm c} - V}{V}\frac{\alpha'}{\beta}}\right), \tag{5}$$

which is for tunneling through an electric n–n junction along the Γ–X direction. When $\theta_0 > \theta_{0c}$, electron beams can be totally reflected at the interface of the junction, since the longitudinal wave vector k'_x in region II becomes imaginary accounting for the occurrence of evanescent modes in the barrier. Based on the obtained results for the transmission probabilities T, one can find the two-terminal Landauer conductance G for the finite structure. Within a linear regime on bias voltage at very low temperatures, the conductance is given by

$$G(E_{\rm F}) = G_0(E_{\rm F})\int_{-\pi/2}^{\pi/2} T\cos\theta_0 d\theta_0, \tag{6}$$

with $G_0 = ge^2 E_{\rm F} L/(h^2 v_{\rm F})$, L is the length of the slab in the transverse direction, and g equals 4 due to the twofold spin and valley degeneracy.

For transport along the Γ–Y direction, due to translation invariance in the x direction, the solution to Eq. (2) in the jth region can be written as $\Psi_j(x,y) = \Psi_j(x)\exp(ik_x x)$. The wavevector k satisfies the relationship $k_{cy}^2 = \frac{(E-E_{\rm c})}{\beta} - \frac{\alpha'}{\beta}k_x^2$, $k_{vy}^2 = \frac{(E_{\rm v}-E)}{\eta} - \frac{\lambda'}{\eta}k_x^2$. The critical angle for tunneling through an electric n–n junction along the Γ–Y direction is

$$\theta_{0c} = \arctan\left(\sqrt{\frac{E - E_{\rm c} - V}{V}\frac{\beta}{\alpha'}}\right). \tag{7}$$

In a similar way, we can also obtain the transmission probability and conductance.

We define

$$\eta = \frac{G_x - G_y}{G_x + G_y}, \tag{8}$$

where G_x (G_y) is the conductance for transport along the Γ–X (Γ–Y) direction.

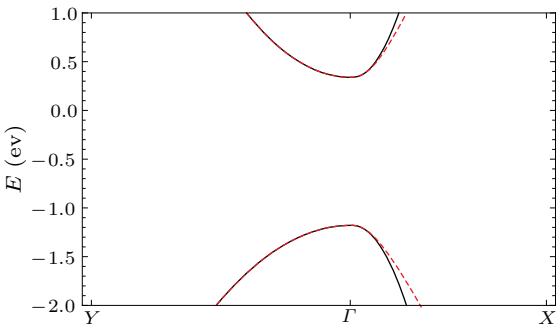

Fig. 2. The energy dispersions of phosphorene, the solid and dashed lines represent the results obtained from the decoupled Hamiltonian (2) and low energy $\boldsymbol{k}\cdot\boldsymbol{p}$ models (1), respectively.

Figure 2 shows the band dispersion of monolayer phosphorene. We can see that the conduction and valence bands are separated by a large energy gap $E_{\rm g} = 1.52\,{\rm eV}$, which is in line with the recent experimental data (1.45 eV).[11] The electronic band structure around the point is an even function of the wave vector as restricted by the symmetry group of the single-layer black phosphorus.[15] We can see that in the energy regime about 300 meV with respect to the band edges, the decoupled Hamiltonian agrees well with the $\boldsymbol{k}\cdot\boldsymbol{p}$ model. Similar to other low-energy $\boldsymbol{k}\cdot\boldsymbol{p}$ models,[1,8] the dispersion expressed by Eq. (2) is strongly anisotropic. The band dispersion is anisotropic in the x–y plane,[13] along the armchair direction the dispersion shows a relativistic-like behavior, while along the zigzag direction there is parabolic dispersion.

Similar to graphene,[16] we can deposit electrostatic gates on the top or back of monolayer phosphorene to create tunable potential barriers. The transmission probability for electrons tunneling through n–n/n–p junctions depends on the incident angle. Figure 3 shows the transmission-angle (T–θ_0) dependence curve along the Γ–X and Γ–Y directions (see the solid black lines and dashed red lines). Figure 3(a) corresponds to transport through an n–n junction, and Fig. 3(b) corresponds to the transport through an n–p junction, respectively. As plotted in Fig. 3, we find that the transmission shows strong anisotropy. For a fixed incident energy, the transmission declines sharply and then is blocked when the incident angle exceeds a critical value θ_{0c}, while the wave vector k_x' in region Ⅱ becomes imaginary, indicating the appearance of evanescent modes. The critical angles for electrons tunneling through n–n junctions for transport along different directions are different (see the solid black lines and dashed red lines in Fig. 3(a)), which can be understood from Eqs. (5) and (7). The width of the gap in the transmission probabilities along the Γ–X direction is larger than that along the Γ–Y direction as the effective masses along the Γ–X direction are smaller than those along the Γ–Y direction (see Eqs. (3) and (4)) in conduction band. For transport through electric n–p junction, the critical value of the incident angle is equal to $\pm\pi/2$.

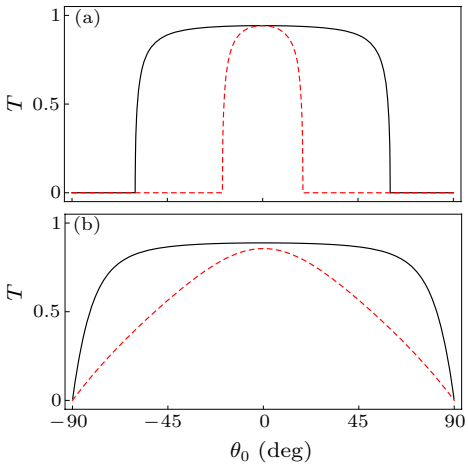

Fig. 3. (Color online) Transmission probability as a function of the incident angle for (a) n–n interface ($E_{\rm F} = 0.5\,{\rm eV}$ and $V = 0.1{\rm eV}$), and (b) n–p interface ($E_{\rm F} = 0.4\,{\rm eV}$ and $V = 1.8\,{\rm eV}$), respectively. The solid lines (dashed lines) are for transport along Γ–X (Γ–Y) direction.

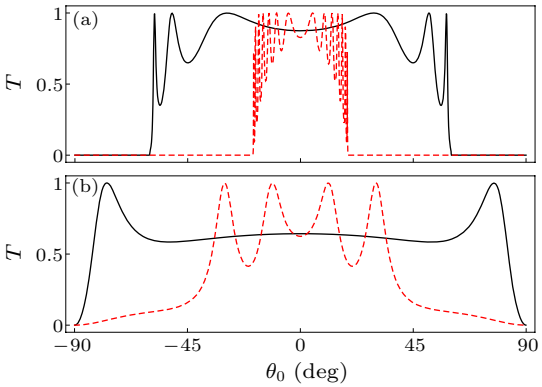

Fig. 4. (Color online) Transmission probability as a function of the incident angle for (a) n–n–n junction ($E_{\rm F} = 0.5\,{\rm eV}$ and $V = 0.1\,{\rm eV}$), (b) n–p–n junction ($E_{\rm F} = 0.4\,{\rm eV}$ and $V = 1.8\,{\rm eV}$), respectively. The barrier width is $D = 20\,{\rm nm}$. The solid black lines (dashed red lines) are for transport along the Γ–X (Γ–Y) direction.

We consider an electric n–p–n channel in the monolayer phosphorene, as shown in Fig. 1. To obtain the transmission probabilities through a single barrier of width D and height V in the x/y direction, we calculate the undetermined coefficients through the application of the boundary conditions, i.e., the wave functions and the first derivative of the wave functions should be continuous at the interface $x = 0$ and $x = D$. The transmission probability for electrons transporting through a barrier depends on the incident angle. Figure 4 shows the transmission-angle dependence for transport along the Γ–X (zigzag) and Γ–Y (armchair) directions. Figure 4(a) corresponds to the transport through an n–n–n junction, and Fig. 4(b) corresponds to transport through an n–p–n junction, respectively. The transmission probability displays oscillating behavior due to the fact that there are the

quasibound states in the well region. When the incident angle exceeds a critical value θ_{0c}, the tunneling is forbidden. This is because the wavevector k'_x becomes imaginary, indicating the appearance of evanescent modes. As seen, the positions of resonant peaks are different for transport along different directions. Here the resonant angles θ_{0m} are determined by $k'_x D = m\pi$ ($m = 1, 2, \ldots$) and $\theta_{0m} \in$ reals, at which the barrier becomes transparent.

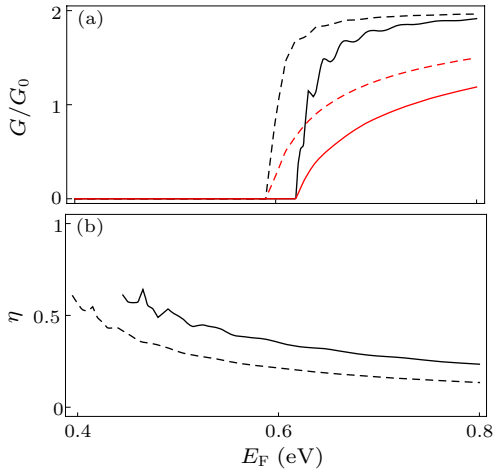

Fig. 5. (Color online) (a) Conductance versus the Fermi energy for transport through a single barrier with barrier heights $V = 0.1$ eV (solid line) and $V = 0.05$ eV (dashed line). The black lines and the red lines are for transport along the Γ–X and Γ–Y directions, respectively. (b) The value of η versus the Fermi energy for transport through a single barrier with barrier heights $V = 0.1$ eV (solid line) and $V = 0.05$ eV (dashed line). The barrier width is $D = 20$ nm.

Finally, we discuss the anisotropic behavior of the conductance. We plot the conductance versus the Fermi energy for transport through a single barrier of width $D = 20$ nm with barrier height $V = 0.1$ eV (solid line) and $V = 0.05$ eV (dashed line) in Fig. 5(a). The width of the gap in the conductance increases with the increasing potential height. At high barrier, the main contribution to the current comes from the evanescent states. At small voltage, we have take into account the propagating waves. This leads to the increase of the conductance. Figure 5(b) shows η as a function of the Fermi energy for transport through different barrier heights. For the smaller incident energy, the anisotropy of the conductance is very large, e.g., approximately 0.6.

In summary, we have investigated theoretically quantum transport of electrons through a single barrier on monolayer phosphorene. Generally, the transmission probability for transport through n–n–n (or n–p–n) junction is an oscillating function of the incident angle, the barrier height, as well as the incident energy of electrons. The transmission probability displays oscillating behavior due to the fact that there are the quasibound states in the well region. The tunneling is forbidden when the incident angle exceeds a critical value. The critical angles for electrons tunneling for transport along different directions, as the different effective masses along Γ–X direction and Γ–Y direction, are different. The positions and the number of resonant peaks depend on the transport direction. Also, we have investigated the conductance for one-dimensional phosphorene single barrier structures. It is found that the conductance shows strong anisotropic behavior, and the width of the gap in the conductance increases with the increasing potential height, which provides us with an efficient way to control the transport of monolayer phosphorene-based microstructures.

References

[1] Rodin A S, Carvalho A and Castro Neto A H 2014 *Phys. Rev. Lett.* **112** 176801

[2] Churchill H O and Jarillo-Herrero P 2014 *Nat. Nanotechnol.* **9** 330

[3] Reich E S 2014 *Nature* **506** 19

[4] Castellanos-Gomez A, Vicarelli L, Prada E, Island J O, Narasimha-Acharya K L, Blanter S I, Groenendijk D J, Buscema M, Steele G A, Alvarez J V, Zandbergen H W, Palacios J J and van der Zant H S J 2014 Two-Dimensional Mater. **1** 025001

[5] Han C Q, Yao M Y, Bai X X, Miao L, Zhu F, Guan D D, Wang S, Gao C L, Liu C, Qian D, Liu Y and Jia J 2014 *Phys. Rev.* B **90** 085101

[6] Lu W, Nan H, Hong J, Chen Y, Zhu C, Liang Z, Ma X, Ni Z, Jin C and Zhang Z 2014 *Nano Res.* **7** 853

[7] Buscema M, Groenendijk D J, Blanter S I, Steele G A, van der Zant H S J and Castellanos-Gomez A 2014 *Nano Lett.* **14** 3347

[8] Low T, Rodin A S, Carvalho A, Jiang Y, Wang Han, Xia F and Castro Neto A H 2014 *Phys. Rev.* B **90** 075434

[9] Rudenko A N and Katsnelson M I 2014 *Phys. Rev.* B **89** 201408

[10] Li L, Yu Y, Ye G J, Ge Q, Ou X, Wu H, Feng D, Chen X H and Zhang Y 2014 *Nat. Nanotechnol.* **9** 372

[11] Liu H, Neal A T, Zhu Z, Luo Z, Xu X, Tománek D and Ye P D 2014 *ACS Nano* **8** 4033

[12] Barbier M, Peeters F M, Vasilopoulos P, Pereira J M and Jr 2008 *Phys. Rev.* B **77** 115446
Barbier M, Vasilopoulos P and Peeters F M 2010 *Philos. Trans. R. Soc.* A **368** 5499
Duppen B V and Peeters F M 2013 *Europhys. Lett.* **102** 27001

[13] Tran V, Soklaski R, Liang Y and Yang L 2014 *Phys. Rev.* B **89** 235319

[14] Zhou X Y, Zhang R, Sun J P, Zou Y L, Zhang D, Lou W K, Cheng F, Zhou G H, Zhai F and Chang K 2015 *Sci. Rep.* **5** 12295

[15] Voon L C L Y, Lopez-Bezanilla A, Wang J, Zhang Y and Willatzen M 2015 *New J. Phys.* **17** 025004

[16] Wu Z H, Zhai F, Peeters F M, Xu H Q and Chang K 2011 *Phys. Rev. Lett.* **106** 176802